A&A 449, 929–935 (2006)
DOI: 10.1051/0004-6361:20053844

Astronomy & Astrophysics

H I observations of galaxies

II. The Coma Supercluster⋆

G. Gavazzi[1], K. O'Neil[2], A. Boselli[3], and W. van Driel[4]

[1] Universitá degli Studi di Milano-Bicocca, Piazza delle scienze 3, 20126 Milano, Italy
e-mail: giuseppe.gavazzi@mib.infn.it
[2] NRAO, PO Box 2, Green Bank, WV 24944, USA
e-mail: koneil@gb.nrao.edu
[3] Laboratoire d'Astrophysique de Marseille, BP 8, Traverse du Siphon, 13376 Marseille, France
e-mail: alessandro.boselli@oamp.fr
[4] Observatoire de Paris, Section de Meudon, GEPI, CNRS UMR 8111 and Université Paris 7, 5 place Jules Janssen, 92195 Meudon Cedex, France
e-mail: wim.vandriel@obspm.fr

Received 18 July 2005 / Accepted 20 September 2005

ABSTRACT

High sensitivity 21-cm H I line observations with an rms noise level of ∼0.5 mJy were made of 35 spiral galaxies in the Coma Supercluster, using the refurbished Arecibo telescope, leading to detection of 25 objects. These data, combined with the measurements available in the literature, provide the set of H I data for 94% of all late-type galaxies in the Coma Supercluster with an apparent photographic magnitude $m_p \leq 15.7$ mag. We confirm that the typical scale of H I deficiency around the Coma cluster is 2 Mpc, i.e. one virial radius. Comparing the H I mass function (HIMF) of cluster with non-cluster members of the Coma Supercluster we detected a shortage of high H I mass galaxies among cluster members that can be attributed to the pattern of H I deficiency found in rich clusters.

Key words. galaxies: distances and redshifts – galaxies: general – galaxies: ISM – galaxies: clusters: individual: Virgo – radio lines: galaxies

1. Introduction

H I line observations of galaxies have provided us with some of the most powerful diagnostics on the role of the environment in regulating the evolution of late-type (spiral) galaxies in the local Universe. Spiral galaxies in rich X-ray luminous clusters display a significant lack of H I gas with respect to their "undisturbed" counterparts in the field (Haynes & Giovanelli 1984; Giovanelli & Haynes 1985). This pattern of H I deficiency can be attributed to various interaction mechanisms: ram-pressure (Gunn & Gott 1972), viscous stripping (Nulsen 1982), thermal evaporation (Cowie & Songaila 1977), or tidal interaction with the cluster potential well (Byrd & Valtonen 1990; Moore et al. 1996). Since these mechanisms have a higher efficiency in or near rich cluster cores, the H I deficiency parameter (Haynes & Giovanelli 1984 – see Sect. 5.1) is an environmental indicator that provides a clear signature of a galaxy's membership in a rich cluster.

The Coma Supercluster has received considerable attention in H I studies due to its proximity to us (∼100 Mpc). Since the pioneering study by Sullivan et al. (1981), various works (e.g. Chincarini et al. 1983a; Gavazzi 1987, 1989; Scodeggio & Gavazzi 1993; Haynes et al. 1997) have provided measurements of the H I content for most late-type galaxies in the Coma Supercluster. In addition to these single-dish studies of their global H I properties, the detailed mapping of galaxies in the Coma and A1367 clusters with radio synthesis telescopes was obtained by Bravo-Alfaro et al. (2000, 2001) and Dickey & Gavazzi (1991).

A high sensitivity, blind H I survey of 7000 square deg. of sky is planned for 2005−2006 with the ALFA multibeam system at Arecibo (Giovanelli et al. 2005), and even more sensitive (1 mJy rms) surveys of parts of these clusters will be obtained with the ALFA system. They will include the Coma Supercluster and the Virgo cluster. In preparation for these surveys, before the installation of the ALFA system, we used the single-beam Arecibo system to continue the pointed observation survey of late-type galaxies in the Virgo cluster (see Gavazzi et al. 2005a, Paper I) and in the Coma Supercluster

⋆ Table 4, Appendix A, Figs. A.1 and A.2 are only available in electronic form at http://www.edpsciences.org

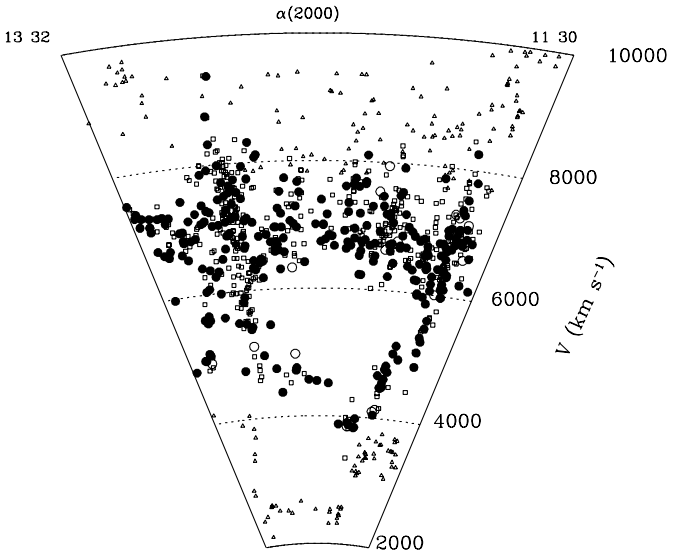

Fig. 1. The wedge diagram of the Coma Supercluster galaxies in the declination interval $18° < \delta < 32°$. Members are divided between late-type (large circles, filled if observed in HI) and early-type (E-S0a: empty squares). Empty triangles mark foreground and background galaxies.

area. Here we report the results of the Coma Supercluster observations that, in conjunction with the previously available H I data-set, enable us to review the properties of galaxies in this Supercluster, as obtained from optically selected H I observations.

The selection of the cluster targets for H I observations is described in Sect. 2, the observations and the data reduction are presented in Sect. 3 and the results are given in Sect. 4 and discussed in Sect. 5. A Hubble constant of 75 km s^{-1} Mpc^{-1} is assumed throughout this paper.

2. Sample selection

Galaxies in the present study were selected from the CGCG Catalogue (Zwicky et al. 1961−68) in the region $11^h30^m < \alpha < 13^h30^m; 18° < \delta < 32°$. There are 1127 CGCG galaxies listed in this region with an apparent photographic magnitude $m_p \leq 15.7$. Their wedge-diagram is given in Fig. 1, where the structure of the Coma–A1367 Supercluster stands out clearly as the pronounced density enhancement near 7000 km s^{-1} and as part of one of the largest known coherent structures in the local universe, named the "Great Wall" (Ramella et al. 1992). Other conspicuous features are: (i) the "Fingers of God" of Coma and A1367, that span the interval $4000 < V < 10\,000$ km s^{-1}, mostly traced by early-type objects, and (ii) the large (∼7500 Mpc^3) "void" in front of the Supercluster, with a density that is 150 times lower than the mean galaxy density in the universe. Other remarkable features, also known as the "legs of the homunculus" (de Lapparent et al. 1986) are two filaments pointing toward the Coma cluster in the interval $4500 < V < 7000$ km s^{-1}. A third "homunculus leg" surrounds the void on the western side, projected near A1367. Objects in the interval $6000 < V < 8000$ km s^{-1} form a bridge between the two clusters with a narrow velocity distribution.

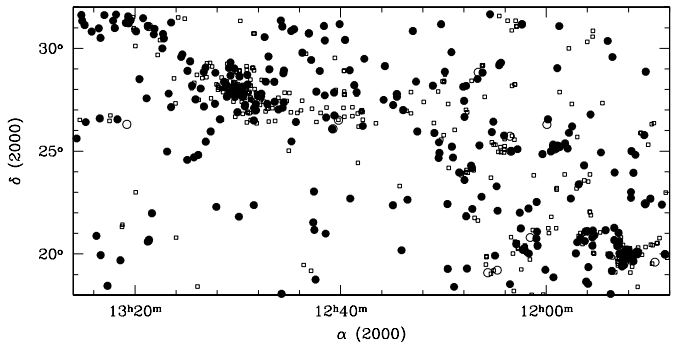

Fig. 2. The sky projection of Coma Supercluster members (including the "homunculus legs" HL). Spirals are represented by circles (filled if observed in H I) and E-S0a objects by empty squares.

Above $V > 8000$ km s^{-1}, the Coma Supercluster fades into the background, so setting a boundary between its members and the projected background objects is rather arbitrary. In assigning the membership of individual galaxies to the various substructures we follow the criteria of Gavazzi et al. (1999).

Out of the 1127 galaxies in Fig. 1, 654 are considered proper Supercluster members according to these criteria, and 76 additional galaxies belonging to the "homunculus legs" (HL) are considered separately (see Table 1). Their sky projection is given in Fig. 2, revealing a substantial morphology segregation between late-type (spiral) and early-type (E-S0a) objects. The Coma Supercluster has also been observed in H I with remarkable completeness: 65% of the published data are found in 5 publications: Chincarini et al. (1983a), Gavazzi (1987, 1989), Scodeggio & Gavazzi (1993), Haynes et al. (1997).

After the present high sensitivity (rms ∼ 0.5 mJy) observations of 33 additional CGCG galaxies (and of two fainter objects: FOCA 610, 636), 295/315 (94%) late-type members (including HL) were observed (see Table 1), of which 259 were detected and 36 have upper limits. Of the remaining 20 unobserved late-type targets, 13 are members of double or multiple systems that could not be resolved by the Arecibo beam (97-111S, 97-129E, 127-051N, 128-029E, 127-025N, 159-049S, 128-031N, 128-002, 97-036, 98-072, 98-073, 98-081, 98-087). The Coma cluster (160-243) and 6 galaxies (127-121, 129-016, 157-077, 158-046, 160-180, 161-029) belonging to the HL were not observed due to scheduling constraints. To fill in a scheduling hole, 13 galaxies in the Virgo cluster were also observed, and all but one were detected. The results of these observations are given in Table 3, and the HI profiles of the detected galaxies are shown in Fig. A.2. These objects will not be considered further in this paper.

All data on the Coma Supercluster and Virgo galaxies are collected and made available worldwide via the "Goldmine" website (`http://Goldmine.mib.infn.it`; see Gavazzi et al. 2003).

3. Observations

Using the refurbished 305-m Arecibo Gregorian radio telescope, we observed 35 galaxies in the Coma Supercluster

Table 1. Sample completeness.

	Type < Sa		Type ≥ Sa	
	All	H I	All	H I
Coma members	391	58	263	249
HL	24	10	52	46
Background	131	5	118	55
Foreground	46	16	102	92
All	592	89	535	442

(plus 13 in the Virgo cluster) (see Sect. 2) in February 2004 and January-March 2005. Data were taken with the *L*-band Wide receiver, using a nine-level sampling with two of the 2048 lag subcorrelators set to each polarization channel. All observations were taken using the position-switching technique, with each blank sky (or OFF) position observed for the same duration, and over the same portion of the telescope dish as the on-source (ON) observation. Each 5 min + 5 min ON+OFF pair was followed by a 10 s ON+OFF observation of a well-calibrated noise diode. The overlaps between both sub-correlators with the same polarization allowed a contiguous radial velocity search range of sufficient width from −1000 to 8500 km s^{-1}. The velocity resolution was 2.6 km s^{-1}, the instrument's *HPBW* at 21 cm is $3\farcm5 \times 3\farcm1$ and the pointing accuracy was about 15″. The pointing positions used were the optical center positions of the target galaxies listed in Table 1. Flux density calibration corrections were good to within 10% (and often much better); see the discussion of the errors involved in O'Neil (2004).

Using standard IDL data reduction software available at Arecibo, corrections were applied for the variations in the gain and system temperature with zenith angle and azimuth. A baseline of order one to three was fitted to the data, excluding those velocity ranges with H I line emission or radio frequency interference (RFI). The velocities were corrected to the heliocentric system, using the optical convention, and the polarizations were averaged. All data were boxcar-smoothed to a velocity resolution of 12.9 km s^{-1} for further analysis. For all spectra, the rms noise level was determined and for the detected objects the central line velocity, the line widths at, respectively, the 50% and 20% level of the peak, and the integrated line flux were determined. No flux correction depending on the source size was applied because the optical extent of all detected targets does not significantly exceed the Arecibo *HPBW*.

4. Results

In order to identify those sources whose H I detections could have been confused by nearby galaxies, we queried the NED, HyperLeda, and Goldmine databases and inspected DSS images over a region of 10′ radius surrounding the central position of each source, given the telescope's sidelobe pattern. Quoted values are weighted averages from the HyperLeda database, unless otherwise indicated.

The H I spectra of both the clearly and the marginally detected galaxies are shown in Figs. A.1 and A.2, and the global H I line parameters are listed in Table 3. These are directly measured values; no corrections have been applied to them for, e.g., instrumental resolution. Table 3 is organized as follows:

Col. 1: Obj. is the galaxy designation;
Cols. 2−3: (J2000) celestial coordinates;
Col. 4: the heliocentric optical recessional velocity (in km s^{-1});
Col. 5: the rms dispersion in the baseline (mJy/beam);
Col. 6: $S_{\rm p}$ is the peak flux density of the detected line (mJy/beam);
Col. 7: $V_{\rm HI}$ is the heliocentric central radial velocity of a line profile (in km s^{-1}) in the optical convention with its estimated uncertainty (see below);
Cols. 8−9: W_{50} and W_{20} are the line widths at 50% and 20% of peak maximum, respectively, (km s^{-1});
Col. 10: $I_{\rm HI}$ is the integrated line flux (Jy km s^{-1}) with its estimated uncertainty (see below);
Col. 11: A quality flag to the spectra is given, where $Q = 1$ stands for high signal-to-noise, double-horned profiles; $Q = 2$ for high signal-to-noise, single-horned profiles; and $Q = 3{,}4$ for low signal-to-noise profiles whose measured line parameters are not reliable. $Q = 5$ is given to unpublished profiles.

We estimated the uncertainties $\sigma_{V_{\rm HI}}$ (km s^{-1}) in $V_{\rm HI}$ and $\sigma_{I_{\rm HI}}$ (Jy km s^{-1}) in $I_{\rm HI}$ following Schneider et al. (1986, 1990), as:

$$\sigma_{V_{\rm HI}} = 1.5(W_{20} - W_{50})X^{-1} \quad (1)$$

and

$$\sigma_{I_{\rm HI}} = 2(1.2W_{20}/R)^{0.5}R\sigma = 7.9(W_{20})^{0.5}\sigma \quad (2)$$

where $I_{\rm HI}$ is the integrated line flux (Jy km s^{-1}), R the instrumental resolution (12.9 km s^{-1}), and X the signal-to-noise ratio of a spectrum, i.e. the ratio of the peak flux density $S_{\rm p}$ and σ, the rms dispersion in the baseline (Jy). The uncertainties in the W_{20} and W_{50} line widths are expected to be 2 and 3 times $\sigma_{V_{\rm HI}}$, respectively.

5. Discussion

The newly obtained H I data were combined with those available from the literature for the $m_{\rm p} \leq 15.7$ late-type galaxies in the Coma Supercluster, as listed in Table 4. The sample comprises 315 galaxies, of which 295 were observed, 259 were detected, and 36 remain undetected. Table 4 is organized as follows:

Col. 1: galaxy designation in the CGCG Catalog;
Col. 2: morphological type;
Col. 3: apparent photographic magnitude from the CGCG;
Col. 4: membership as defined in Gavazzi et al. (1999). Distances D of 96.0 and 91.3 Mpc are assumed for Coma and A1367, respectively. Distances of individual groups and substructures in the Great Wall (including HL) are taken from Gavazzi et al. (1999) (rescaled to $H_0 = 75$ km s^{-1} Mpc^{-1}). Distances from individual redshifts are assumed for supercluster isolated galaxies and members of multiplets;

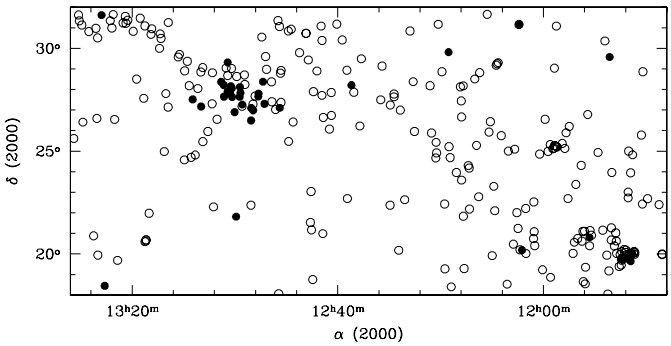

Fig. 3. The late-type Coma Supercluster members (including HL) coded according to their H I deficiency parameter: $\mathrm{Def_{HI}} \leq 0.5$ (empty circles); $\mathrm{Def_{HI}} > 0.5$ (filled circles).

Col. 5: recessional velocity in km s^{-1};

Col. 6: H I mass or mass limit in solar units: $M_{\rm HI} = 2.36 \times 10^5 D^2\ I_{\rm HI}$. For undetected galaxies, we set $I_{\rm HI} = 1.5 \times \mathrm{rms_{HI}} \times W_{\langle 20-50 \rangle}$, where $\mathrm{rms_{HI}}$ is the rms of the spectra in mJy, and the $W_{\langle 20-50 \rangle}$ profile width is based on the following average line widths of the detected objects per Hubble type bin: 300 km s^{-1} for Sa-Sbc, 190 km s^{-1} for Sc-Scd;

Col. 7: coded reference to the H I measurement (see the notes to the table);

Col. 8: H I deficiency parameter as defined in Haynes & Giovanelli (1984) (see Sect. 5.1);

Col. 9: quality flag (see last column of Table 3).

5.1. The pattern of H I deficiency

For the late-type galaxies in the present study, we estimated the H I deficiency parameter following Haynes & Giovanelli (1984) as the logarithmic difference between $M_{\rm HI}$ of a reference sample of isolated galaxies and $M_{\rm HI}$ as actually observed in individual objects: $\mathrm{Def_{HI}} = \mathrm{Log}M_{\rm HI\ ref.} - \mathrm{Log}M_{\rm HI\ obs.}$. Then, $M_{\rm HI\ ref}$ is computed from the galaxies optical linear diameter d as: $\mathrm{Log}M_{\rm HI\ ref} = a + b\mathrm{Log}(d)$, where d is estimated consistently with Haynes & Giovanelli (1984); and a and b are weak functions of the Hubble type, as listed in Table 3 of Paper I (notice that $b \sim 2$ across the Hubble sequence, i.e. $M_{\rm HI\ ref}$ increases approximately as the galaxy linear diameter squared).

Figure 3 shows that H I deficient galaxies segregate around the center of the Coma cluster and, to a much lesser degree, around A1367. One important issue that can be addressed with the present data-set, given its completeness, is on what scale the phenomenon of H I ablation holds. The H I deficiency parameter of individual galaxies is given in Fig. 4 as a function of the projected linear separation from the X-ray center of the Coma cluster, out to 15 Mpc, along with average values taken in bins of 0.5° (from 0° to 2°) and in bins of 1° further out (see also Table 2). It is apparent that significant H I deficiency occurs out to approximately 3 Mpc radius. At one virial radius (i.e. at 2.2 Mpc, Girardi et al. 1998; or 2.9 Mpc Lokas & Mamon 2003; Neumann et al. 2001), the average H I content of the supercluster galaxies becomes indistinguishable from that of the field, in agreement with Solanes et al. (2001)[1].

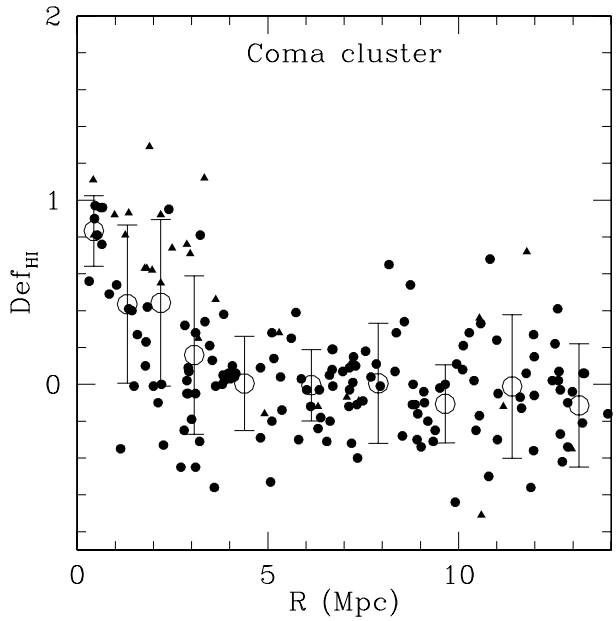

Fig. 4. The projected distribution about the X-ray center of the Coma cluster of the H I deficiency of Late-type Supercluster detected (dots) and undetected (triangles) members (excluding HL). Large circles represent averages in bins of 0.5° (1°). One σ errorbars are given.

Table 2. The radial distribution of the mean binned H I deficiency of Late-type Supercluster members (excluding HL) about the Coma cluster.

Θ(Deg.)	R (Mpc)	$\langle \mathrm{Def_{HI}} \rangle$
0.0–0.5	0.42	0.83 ± 0.19
0.5–1.0	1.25	0.43 ± 0.43
1.0–1.5	2.09	0.44 ± 0.45
1.5–2.0	2.93	0.16 ± 0.43
2.0–3.0	4.19	0.00 ± 0.25
3.0–4.0	5.87	0.00 ± 0.19
4.0–5.0	7.55	0.00 ± 0.32
5.0–6.0	9.24	–0.10 ± 0.21
6.0–7.0	10.9	–0.01 ± 0.39
7.0–8.0	12.6	–0.11 ± 0.33

The star-formation rate, as derived from Hα observations, shows a significant cut-off near 1 to 2 projected virial radii from the Coma cluster (Gavazzi et al. 2005b) and from overdensity peaks in the SDSS (Nichol 2004; Miller 2004). What the H I observations show is the driver of the SFR decline, i.e. the lack of gas to sustain it.

[1] Galaxies in the HL, identified as such outward of 2° from Coma and A1367, on average do not show significant deficiency are not included in Fig. 4.

Table 3. Parameters of the newly observed galaxies.

Obj.	RA	Dec	V_{opt}	σ	S_p	V_{HI}	W_{50}	W_{20}	I_{HI}	Qual.
	J2000.0		km s^{-1}	mJy/beam	mJy/beam	km s^{-1}	km s^{-1}	km s^{-1}	Jy km s^{-1}	
Coma Supercluster										
CGCG 97-078	114316.24	194455.6	7560 ± 70	0.54	–	–	–	–	–	–
CGCG 127-018	113944.62	224107.7	–	0.56	17.0	6922 ± 2	147	168	2.09 ± 0.06	1
CGCG 127-039	114330.88	230043.3	6908 ± 60	0.62	22.4	6911 ± 1	37	58	0.82 ± 0.04	2
CGCG 97-124	114456.97	194353.9	7771 ± 60	0.66	–	–	–	–	–	–
CGCG 127-055	114646.66	211616.9	6615 ± 52	0.67	9.3	6626 ± 3	215	242	1.86 ± 0.08	1
CGCG 127-067	115039.40	205426.1	6349 ± 39	0.43	3.8	6400 ± 16	283	304	0.73 ± 0.10	1
CGCG 157-044	115123.19	264703.6	6624 ± 44	0.64	5.1	6607 ± 4	240	260	0.84 ± 0.08	1
CGCG 97-172	115214.30	183905.7	7650 ± 56	0.36	1.6	7826 ± 16	214	227	0.21 ± 0.10	3
CGCG 127-137W	120141.90	202417.3	6794	0.49	3.4	6871 ± 16	357	398	1.07 ± 0.10	1
CGCG 98-023	120144.40	175353.8	6905 ± 48	0.38	5.8	6905 ± 16	262	282	1.01 ± 0.10	1
CGCG 127-136	120147.40	210506.7	6930	0.29	17.5	6675 ± 16	173	228	2.36 ± 0.10	2
CGCG 127-138	120155.47	204452.1	7192 ± 46	0.60	–	–	–	–	–	–
CGCG 128-015	120456.20	211427.5	6729 ± 16	0.44	19.0	6741 ± 16	102	124	1.64 ± 0.10	2
CGCG 99-002	121755.86	182357.8	7640 ± 59	0.90	2.7	(7605)	–	–	–	4
CGCG 128-072	121808.27	244118.5	6838 ± 51	0.63	8.3	6795 ± 6	119	174	0.82 ± 0.07	1
CGCG 99-013	121910.00	191626.9	7297 ± 16	0.36	7.2	7336 ± 16	235	251	1.41 ± 0.10	1
CGCG 128-081	122052.50	252547.2	7112	0.42	5.0	7204 ± 16	290	312	1.00 ± 0.10	1
CGCG 129-004	122949.40	222219.4	6847 ± 70	0.57	5.5	6736 ± 7	275	317	1.09 ± 0.08	1
CGCG 159-048	124011.35	311038.1	7096 ± 44	0.65	7.0	7064 ± 8	309	363	1.60 ± 0.10	1
CGCG 159-071	124543.41	292558.5	6936 ± 44	1.06	17.1	6971 ± 1	189	202	2.60 ± 0.10	1
CGCG 159-097	125206.77	270134.3	6573 ± 190	0.65	3.2	6424 ± 30	260	357	0.60 ± 0.10	3
CGCG 160-009	125432.95	282234.7	7079 ± 63	0.70	–	–	–	–	–	–
FOCA 636	125756.70	275930.0	4649	0.40	1.8	4605 ± 30	130	219	0.18 ± 0.05	3
FOCA 610	125757.70	280342.0	8299	0.38	1.7	8125 ± 8	211	236	0.19 ± 0.05	3
CGCG 130-003	125947.24	214845.7	7094 ± 32	0.55	4.4	7140 ± 4	335	357	0.51 ± 0.08	3
CGCG 160-261	130059.10	275358.6	6896 ± 7	0.37	–	–	–	–	–	–
CGCG 160-128	130422.57	284838.5	8054 ± 36	0.74	25.7	7920 ± 1	115	137	2.46 ± 0.07	1
CGCG 160-138	130635.52	271006.2	7852 ± 60	0.37	–	–	–	–	–	–
CGCG 160-146	130814.00	273055.3	7337 ± 23	0.25	–	–	–	–	–	–
CGCG 160-169	131440.60	295951.8	6960 ± 60	0.69	6.2	6850 ± 4	298	318	1.26 ± 0.10	1
CGCG 130-029	131730.80	203555.1	6671 ± 71	0.36	4.6	6560 ± 16	317	325	1.30 ± 0.10	1
CGCG 160-195	131947.60	304931.9	7297 ± 15	0.34	5.0	7247 ± 16	158	223	0.63 ± 0.10	2
CGCG 161-048	132557.14	313703.6	7268 ± 44	0.66	–	–	–	–	–	–
CGCG 161-051	132643.29	303026.7	7150 ± 60	1.52	–	–	–	–	–	–
CGCG 161-054	132703.07	305834.3	7668 ± 44	0.62	7.0	6756 ± 3	284	303	1.34 ± 0.09	1
Virgo Cluster										
VCC 30	121054.50	155654.6	–	0.92	9.5	2084 ± 16	116	148	0.83 ± 0.10	2
VCC 85	121336.50	130201.1	–	0.32	2.4	1932 ± 16	74	84	0.14 ± 0.10	2
VCC 113	121432.90	120612.0	2155	0.33	17.5	2091 ± 16	148	171	2.12 ± 0.10	2
VCC 137	121508.60	145819.5	–	0.56	–	(4000)	–	–	–	4
VCC 429	122044.20	143803.3	–	0.39	4.0	600 ± 16	87	109	0.27 ± 0.10	2
VCC 578	122243.60	183252.1	–	0.39	4.0	6490 ± 16	161	178	0.48 ± 0.10	1
VCC 1574	123432.90	151052.3	–	0.17	2.3	639 ± 16	127	161	0.22 ± 0.10	2
VCC 1623	123531.90	163646.9	–	0.30	1.9	2108 ± 16	78	91	0.13 ± 0.10	2
VCC 1821	124008.90	065302.1	–	0.31	2.5	1007 ± 16	75	87	0.16 ± 0.10	2
VCC 1873	124118.60	063127.0	–	0.26	17.0	1692 ± 16	112	134	1.37 ± 0.10	2
VCC 1898	124157.50	034909.4	881 ± 23	0.50	–	–	–	–	–	–
VCC 2071	124825.40	091856.8	–	0.32	2.7	6484 ± 16	185	196	0.40 ± 0.10	2
CGCG 43066	125515.40	025348.4	2798 ± 23	0.47	21.0	2802 ± 16	382	403	6.09 ± 0.10	1

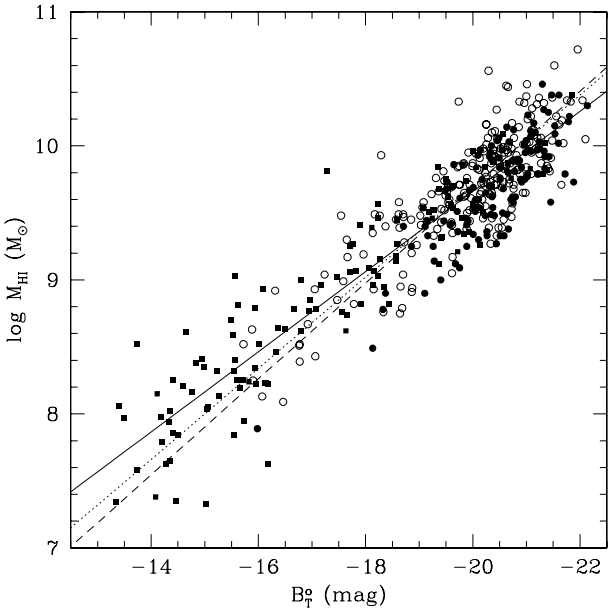

Fig. 5. The correlation between $\log M_{\rm HI}$ and $B^{\circ}_{\rm T}$ for Sa-Sb (filled circles), Sbc-Sc (empty circles), Scd-Im-BCD (filled squares). The direct fit (solid line), the inverse fit (dashed) (obtained considering all Hubble types), and the relation used in Paper I (dotted) are given.

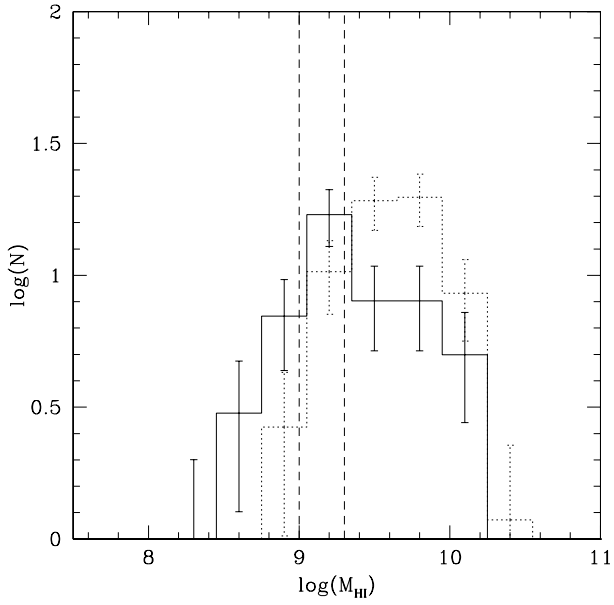

Fig. 6. The MHI function for the members of the Coma+A1367 clusters (solid) and for the non-cluster Supercluster members (dotted). The optical ($\log M_{\rm HI} = 9.3\ M_{\odot}$) and radio ($\log M_{\rm HI} = 9.0\ M_{\odot}$) completeness limits are drawn.

5.2. The H I mass–B°_{T} relation

Taking advantage of the large sample of optically selected galaxies with H I measurements and optical (B-band) photometry (accurate to within 0.1 mag), we study the H I mass vs. $B^{\circ}_{\rm T}$ relation for unperturbed galaxies. However, since the Coma Supercluster sample ($m_{\rm p} \leq 15.7$) contains only giant galaxies brighter than $M_{\rm p} = -19.1$, we have included the Virgo galaxies (Paper I) for the purpose of extending this correlation over a broader magnitude range. In doing so we must obviously exclude galaxies with perturbed H I contents. Conservatively, we excluded galaxies with $\rm Def_{HI} \geq 0.2$ (the $\rm Def_{HI}$ parameter is determined from diameters (Sect. 5.1), independent of the B luminosity, as in Haynes & Giovanelli 1984). Figure 5 shows the relation for the 465 late-type galaxies that were selected accordingly, and plotted in three bins of Hubble type to stress the consistency among them. The three given linear regressions, obtained combining all Hubble types, are the direct one ($M_{\rm HI} = 3.680 - 0.299 \times M_{\rm p}$), the inverse one ($M_{\rm p} = 7.090 - 2.795 \times M_{\rm HI}$), and the one adopted in Paper I ($M_{\rm HI} = 2.9 - 0.34 \times M_{\rm p}$). The residual of the (direct) correlation is $\sigma(\log M_{\rm HI}) = 0.26$; i.e., the H I mass of disk galaxies can be predicted within a factor of 1.8 uncertainty from their B luminosity.

5.3. The H I mass function

Figure 6 shows the frequency distribution of $M_{\rm HI}$ for the cluster (Coma + A1367) late-type galaxies (solid histogram) and for the isolated galaxies (including HL), the latter normalized to the former by the ratio of the number of galaxies. The H I Mass Function (HIMF) so obtained cannot be meaningfully compared with the one of Virgo, obtained in Paper I, or even with the one of isolated galaxies by Zwaan et al. (2003), because of the shallowness of the optical and 21 cm observations available for the Coma Supercluster. Given the relation $M_{\rm HI} = 3.680 - 0.299 \times M_{\rm p}$, discussed in the previous section, the limiting magnitude $m_{\rm p} \leq 15.7$ ($M_{\rm p} \geq -19.1$) of the CGCG implies that, on average, only galaxies with $\log M_{\rm HI} > 9.3\ M_{\odot}$ are targeted. This imposes a completeness cut-off that is even shallower than the limiting detectable H I mass of $\log M_{\rm HI} > 9.0\ M_{\odot}$ that derives from the typical noise figure of the 21 cm observations ($\langle\sigma\rangle \sim 1$ mJy). In Paper I we showed that significant differences between the HIMF of the Virgo cluster and of the field occur for $\log M_{\rm HI} < 9.0\ M_{\odot}$, i.e. below both the present cut-off lines. For $9.5 < \log M_{\rm HI} < 10\ M_{\odot}$, however, there is in Fig. 6 a barely significant excess in the frequency of non-cluster members of the Coma Supercluster with respect to cluster members. This can be understood as a signature of the deficiency pattern of cluster galaxies, as found in Paper I for Virgo.

6. Summary and conclusions

We observed 35 galaxies in the Coma Supercluster and 13 in the Virgo cluster in the 21-cm H I line with the refurbished Arecibo telescope. The high sensitivity of our observations (rms noise ∼0.5 mJy) resulted in the detection of 37 objects, and significant upper limits were obtained for the remaining ones. Including the present observations, the H I survey of the Coma Supercluster has reached virtual completion (94% among the late-type members). And, by combining all data, we have determined with high significance that the typical scale of H I deficiency around the Coma cluster is 2−3 Mpc, i.e. one virial radius.

With the present data, a meaningful determination of the HIMF can be only obtained for $\log M_{\rm HI} > 9.0\ M_{\odot}$, insufficient for comparing it with the deeper HIMF of Virgo (Paper I)

and of isolated galaxies (Zwaan et al. 2003). Comparing cluster with non-cluster Supercluster members, we do, however, detect a shortage of high H I mass galaxies among cluster members which can be attributed to the pattern of H I deficiency found in rich clusters.

Acknowledgements. The Arecibo Observatory is part of the National Astronomy and Ionosphere Center, which is operated by Cornell University under a cooperative agreement with the National Science Foundation. This research also made use of the Lyon-Meudon Extragalactic Database (LEDA), recently incorporated in HyperLeda and the NASA/IPAC Extragalactic Database (NED), operated by the Jet Propulsion Laboratory, California Institute of Technology, under contract with the National Aeronautics and Space Administration and the Goldmine database.

References

Beijersbergen, M. 2003, Ph.D. Thesis, Groningen University
Binggeli, B., Sandage, A., & Tammann, G. A. 1985, AJ, 90, 1681 (VCC)
Bothun, G., Aaronson, M., Schommer, R., Mould, J., Huchra, J., & Sullivan, W. 1985, ApJS, 57, 423
Bravo-Alfaro, H., Cayatte, V., van Gorkom, J. H., & Balkowski, C. 2000, AJ, 119, 580
Bravo-Alfaro, H., Cayatte, V., van Gorkom, J. H., & Balkowski, C. 2001, A&A, 379, 347
Byrd, G., & Valtonen, M. 1990, ApJ, 350, 89
Chincarini, G., Giovanelli, R., & Haynes, M. P. 1983a, ApJ, 269, 13
Chincarini, G., Giovanelli, R., Haynes, M., & Fontanelli, P. 1983b, ApJ, 267, 511
Cowie, L. L., & Songaila, A. 1977, Nature, 266, 501
de Lapparent, V., Geller, M. J., & Huchra, J. P. 1986, ApJ, 302, L1
Dell'Antonio, I., Bothun, G., & Geller, M. 1996, AJ, 112, 1759
Dickey, J. M., & Gavazzi, G. 1991, ApJ, 373, 347
Eder, J., Giovanelli, R., & Haynes, M. 1991, AJ, 102, 572
Fontanelli, P. 1984, A&A, 138, 85
Gavazzi, G. 1987, ApJ, 320, 96
Gavazzi, G. 1989, ApJ, 346, 59
Gavazzi, G., Carrasco, L., & Galli, R. 1999, A&AS, 136, 227
Gavazzi, G., Boselli, A., Donati, A., Franzetti, P., & Scodeggio, M. 2003, A&A, 400, 451
Gavazzi, G., Boselli, A., van Driel, W., & O'Neil, K. 2005a, A&A, 429, 439 (Paper I)
Gavazzi, G., Boselli, Cortese, L., Arosio, I., et al. 2005b, A&A, submitted
Giovanelli, R., & Haynes, M. 1985, ApJ, 292, 404
Giovanelli, R. 2005, AJ, in press
Girardi, M., Giuricin, G., Mardirossian, F., Mezzetti, M., & Boschin, W. 1998, ApJ, 505, 74
Gunn, J. E., & Gott, J. R. III 1972, ApJ, 176, 1
Haynes, M., & Giovanelli, R. 1984, AJ, 89, 758
Haynes, M., Giovanelli, R., & Chincarini, G. 1984, ARA&A, 22, 445
Haynes, M., Giovanelli, R., Herter, T., et al. 1997, AJ, 113, 1197
Lewis, B., Helou, G., & Salpeter, E. 1985, ApJS, 59, 161
Lokas, E. L., & Mamon, G. A. 2003, MNRAS, 343, 401
Lu, N., Hoffman, G. L., Groff, T., Ross, T., & Lamphier, C., 1993, ApJS, 88, 383
Magri, C. 1994, AJ, 108, 896
Miller, C. J. 2004, in Clusters of Galaxies: Probes of Cosmological Structure and Galaxy Evolution, from the Carnegie Observatories Centennial Symposia (Cambridge University Press), as part of the Carnegie Observatories Astrophysics Series, ed. J. S. Mulchaey, A. Dressler, & A. Oemler
Moore, B., Katz, N., Lake, G., Dressler, A., & Oemler, A., Jr. 1996, Nature, 379, 613
Mould, J., Martin, S., Bothum, G., Huchra, J., & Shomma, B. 1995, ApJS, 96, 1
Neumann, D. M., Arnaud, M., Gastaud, R., et al. 2001, A&A, 365, L74
Nichol, R. C. 2004, in Clusters of Galaxies: Probes of Cosmological Structure and Galaxy Evolution, from the Carnegie Observatories Centennial Symposia (Cambridge University Press), part of the Carnegie Observatories Astrophysics Series, ed. J. S. Mulchaey, A. Dressler, & A. Oemler, 24
Nulsen, P. E. J. 1982, MNRAS, 198, 1007
O'Neil, K. 2004, AJ, 128, 2080
Ramella, M., Geller, M. J., & Huchra, J. P. 1992, ApJ, 384, 396
Salzer, J., Hanson, M., & Gavazzi, G. 1990, ApJ, 353, 39
Scodeggio, M., & Gavazzi, G. 1993, ApJ, 409, 110
Solanes, J., Manrique, A., Garcia-Gómez, C., et al. 2001, ApJ, 548, 97
Sulentic, J., & Arp, H. 1982, AJ, 88, 489
Sullivan III, W. T., Bothun, G. D., Bates, B., & Schommer, R. A. 1981, AJ, 86, 919
van Driel, W., Ragaigne, D., Boselli, A., Donas, J., & Gavazzi, G. 2000, A&AS, 144, 463
Vogt, N. P., Haynes, M. P., Herter, T., & Giovanelli, R. 2004, AJ, 127, 3273
Williams, B., & Kerr, F. 1981, AJ, 86, 953
Zwaan, M. A., Staveley-Smith, L., Korivalski, B., et al. 2003, AJ, 125, 2842

Online Material

Table 4. Basic H I properties of late-type members to the Coma Supercluster (including HL).

CGCG	Type	m_p mag	Cloud	V km s^{-1}	log M_{HI} $M_\odot$	Ref.	Def$_{HI}$	Qual
097-005	Sc	15.5	Isol.	6129	9.72	126	–0.29	1
097-026	Pec	13.9	Pair	6202	9.88	39	–0.45	1
097-027	Sc	14.6	Pair	6630	9.27	24	0.28	2
097-036	S..	15.7	Pair	6595	–	–	–	–
097-062	Pec	15.5	A1367	7809	9.33	40	0.31	1
097-063	Pec	15.7	A1367	6102	9.09	24	0.22	2
097-064	S..	15.6	A1367	5976	9.17	126	0.03	3
097-068	Sbc	14.7	A1367	5974	9.99	126	–0.14	1
097-072	Sa	15.0	A1367	6332	9.14	126	0.50	1
097-073	Pec	15.6	A1367	7290	9.31	40	0.16	2
097-076	Sb	15.5	A1367	7060	<8.39	40	>1.39	–
097-078	Sa	15.2	A1367	7526	<8.68	193	>1.28	–
097-079	Pec	15.7	A1367	6996	9.21	40	0.25	1
097-082	Sa	15.0	A1367	6100	<8.68	2	>1.01	5
097-087	Pec	14.3	A1367	6735	9.83	40	0.19	1
097-091	Sa	14.7	A1367	7368	9.77	126	–0.18	1
097-092	Sbc	15.5	A1367	6373	9.18	24	0.31	4
097-093	Pec	15.5	A1367	4857	9.03	4	0.57	4
097-102N	Sa	15.1	A1367	6361	9.21	40	0.36	1
097-111S	Pec	16.5	A1367	7239	–	–	–	–
097-114	Pec	15.4	A1367	8257	9.44	193	–0.17	1
097-119	Sa	15.7	A1367	5256	8.92	4	0.22	1
097-120	Sa	14.5	A1367	5595	8.80	4	0.90	4
097-121	Sab	14.6	A1367	6571	9.37	126	0.28	1
097-122	Pec	14.9	A1367	5468	9.35	126	0.49	1
097-129E	Sbc	15.7	A1367	6009	–	–	–	–
097-129W	Sb	14.0	A1367	5082	10.09	24	0.18	1
097-130	Sa	15.5	A1367	6697	<8.83	1	>0.40	5
097-138	Pec	15.5	A1367	5317	9.69	40	–0.22	3
097-149	S..	15.6	A1367	6060	<9.25	105	>0.07	–
097-151	Sab	15.6	Isol.	5854	9.05	88	0.34	1
097-152	Sa	15.5	A1367	6166	9.40	126	0.23	1
097-168	S..	15.7	Isol.	5996	<8.91	88	>0.25	–
097-169	Sc	15.7	Pair	5975	9.45	6	0.05	2
097-172	S..	15.7	Pair	7826	8.71	193	0.38	3
098-002	Sb	15.6	Isol.	6206	9.41	88	0.10	1
098-007	Sbc	15.5	Isol.	6350	9.86	88	–0.30	1
098-013	Sc	15.1	Isol.	6949	9.65	40	–0.12	1
098-016	Sc	15.3	Isol.	6449	9.72	15	0.11	1
098-017	Sbc	15.7	Isol.	7015	9.66	40	0.05	2
098-023	Sb	15.1	Tripl.	6905	9.30	193	–0.01	1
098-034	S..	14.8	N4065 G	6432	9.07	40	0.11	3
098-041	Sc	15.7	N4065 G	7551	9.28	24	0.65	2
098-046	Sa	14.3	N4065 G	6220	9.58	24	0.07	1
098-050	Sc	14.1	IC202 HL	4372	9.44	24	–0.04	1
098-051	Sa	14.6	IC202 HL	4283	9.6	88	–0.35	4
098-058	Sbc	14.7	Isol.	7207	9.95	24	0.00	1
098-067	S..	15.7	Isol.	7610	<9.64	184	>–0.71	–
098-071	Pec	15.5	Pair	6881	9.62	184	–0.05	1
098-072	S..	15.7	Pair	7946	–	–	–	–
098-073	Sb	15.7	Tripl.	6440	–	–	–	–
098-074	Sa	15.6	Isol.	7471	<9.10	88	>0.36	–
098-081	Sa	15.2	Pair	7177	–	–	–	–
098-085	Sc	14.7	Tripl.	7042	9.69	24	–0.13	2
098-087	S..	15.3	Pair	7540	–	–	–	–
098-116	Sc	14.9	Isol.	6229	9.91	24	–0.34	1
099-002	S..	15.5	Isol.	7605	9.02	193	–0.08	3
099-013	Sc	15.7	Isol.	7736	9.50	193	–0.40	1

Table 4. continued.

CGCG	Type	m_p mag	Cloud	V km s^{-1}	log M_{HI} $M_\odot$	Ref.	Def$_{HI}$	Qual
100-005	Pec	14.4	Isol.	6611	9.37	24	0.41	1
100-012	Pec	15.3	Isol.	6481	9.32	24	–0.12	2
101-033	Sc	15.7	Isol.	6729	9.68	43	0.07	1
101-043	Sa	15.0	Isol.	6677	<8.74	88	>0.96	–
101-049	Sbc	14.9	Isol.	7148	10.06	7	–0.24	2
101-054	Sab	13.8	Isol.	6606	9.92	24	–0.20	3
127-005	Sbc	15.4	Isol.	6864	9.64	6	0.04	2
127-018	Sb	15.0	Isol.	6922	9.63	193	–0.14	1
127-025N	Sc	15.3	Pair	7142	–	–	–	–
127-025S	Sbc	14.5	Pair	7076	9.87	126	0.09	1
127-026	Sbc	14.8	Isol.	6871	9.95	24	–0.17	1
127-033	Sc	15.2	Isol.	6300	9.77	24	0.00	1
127-035	Sa	15.4	Isol.	6817	9.49	88	0.15	1
127-037	Pec	15.4	Isol.	6186	9.54	24	–0.10	2
127-038	Sc	14.0	Isol.	6913	10.36	2	–0.20	1
127-039	Sbc	15.3	Isol.	6911	9.21	193	0.25	2
127-049	Pec	15.5	A1367	7061	9.34	6	0.32	1
127-050	Sbc	14.8	N3937 G	6752	9.95	2	0.00	1
127-051N	Pec	15.8	A1367	7288	–	–	–	–
127-052	Sa	14.0	A1367	6946	9.73	126	0.16	1
127-053	Sbc	15.4	Isol.	6409	1 –	24	–0.11	1
127-054	Sb	14.2	N3937 G	7026	10.38	2	0.10	1
127-055	Pec	15.1	Isol.	6626	9.54	193	–0.45	1
127-056	Sb	15.7	Isol.	6814	9.67	126	–0.05	1
127-061	Sc	15.4	Isol.	5954	9.85	24	–0.20	1
127-067	S..	15.5	N3937 G	6400	9.18	193	–0.31	1
127-071	Pec	15.4	N3937 G	6388	9.36	24	0.13	2
127-072	Sc	14.6	N3937 G	6438	9.89	3	–0.05	1
127-073	Sb	15.1	N3937 G	6439	9.01	1	0.81	4
127-082	Sc	14.7	N3937 G	6654	9.47	2	0.02	2
127-083	Sbc	15.1	N3937 G	6743	9.39	6	0.06	3
127-085	Sa	15.5	N3937 G	6595	<8.99	88	>0.46	–
127-087	Sbc	15.4	N4005 HL	4941	9.66	126	0.05	1
127-095	Sc	14.2	N3937 G	6199	10.04	2	0.03	1
127-099	Sc	14.5	Pair	6458	9.71	126	0.10	1
127-100	Sb	14.9	N3937 G	6854	9.58	2	0.06	3
127-104	Sbc	15.5	Isol.	6814	9.63	6	0.19	1
127-106	Sb	14.5	N4005 HL	5027	9.88	24	–0.32	1
127-107	Sbc	15.7	Isol.	6355	9.36	126	0.02	3
127-109	Sbc	15.7	N4005 HL	4731	9.4	32	–0.04	2
127-110	Sbc	14.4	N4005 HL	4495	9.81	24	0.22	1
127-111	Sbc	15.7	N4005 HL	4617	9.47	111	–0.41	1
127-112	Sbc	14.8	N4005 HL	4828	9.63	32	0.25	1
127-114E	Pec	15.0	N4005 HL	4771	9.84	24	–0.02	3
127-114W	Pec	15.0	N4005 HL	4771	9.84	24	–0.13	3
127-118	Sc	15.2	N4005 HL	4551	9.38	24	0.13	1
127-120	Sb	14.1	N4005 HL	4470	9.32	24	0.22	3
127-121	Sb	15.7	N4005 HL	4131	–	–	–	–
127-123	Sc	14.7	N4005 HL	4479	9.84	24	–0.03	1
127-127	Sb	14.6	N4005 HL	4048	9.34	111	0.14	1
127-133	Sc	15.3	N4005 HL	4667	9.12	32	–0.08	1
127-136	S..	15.7	Pair	6675	9.68	193	–1.02	2
127-137W	S..	16.0	N4065 G	6871	9.38	193	–0.32	1
127-138	S..	15.5	Isol.	7210	<8.77	193	>–0.09	–
127-139	Sa	15.5	Isol.	6713	9.29	24	0.34	3
128-002	S..	15.7	N4065 G	6780	–	–	–	–
128-003	Pec	14.6	Isol.	6435	9.69	2	–0.11	2
128-015	Sb	15.3	Pair	6741	9.51	193	–0.11	2

Table 4. continued.

CGCG	Type	m_p mag	Cloud	V km s^{-1}	log M_{HI} $M_\odot$	Ref.	Def_{HI}	Qual
128-016	S..	15.2	Isol.	6619	9.30	24	–0.31	1
128-021	Sbc	15.4	Isol.	7064	9.83	24	0.02	1
128-023	Sa	14.4	N4065 G	6719	9.92	2	–0.30	1
128-029E	S..	16.7	IC762 G	6634	–	–	–	–
128-029W	S..	16.2	IC762 G	7158	9.39	40	–0.10	3
128-031N	S..	16.5	Isol.	6936	–	–	–	–
128-037	Sbc	14.8	IC762 G	7194	9.53	2	0.11	2
128-042N	S..	16.3	Isol.	7319	9.78	43	–0.30	3
128-044	S..	15.7	Isol.	6922	10.25	7	–0.36	1
128-049	Sc	15.0	Isol.	6445	9.21	24	0.49	4
128-052	Sb	15.6	Isol.	6692	9.48	22	0.07	2
128-053	Sbc	15.6	Isol.	7307	10.06	40	0.01	1
128-057	S..	15.6	Isol.	6998	<9.51	184	>–0.35	–
128-058	S..	15.7	N4213 G	6778	9.52	7	–0.25	2
128-059	Sb	15.6	N4213 G	6228	9.95	7	–0.28	1
128-063	Sa	15.3	Pair	6747	9.97	24	0.06	1
128-066	S..	15.1	N4213 G	6526	<9.11	88	>0.34	–
128-069	Sbc	15.6	N4213 G	7188	9.16	111	0.28	2
128-072	Pec	15.4	Isol.	6795	9.21	193	0.02	1
128-073	Sb	14.7	Isol.	6948	9.96	126	0.01	1
128-075	Sc	15.5	Isol.	6682	9.93	126	0.10	3
128-079	Sc	15.6	Isol.	6630	9.71	40	–0.25	2
128-080	Sb	15.0	Isol.	7349	9.38	24	0.05	3
128-081W	S..	16.5	Isol.	7204	9.33	193	–0.29	1
128-082	Sb	15.7	Isol.	6910	1 –	111	–0.05	1
128-087	Sc	15.3	Isol.	6671	9.55	5	0.13	1
128-089	Sa	14.2	Isol.	6841	9.23	40	0.35	3
128-090	Sc	15.5	Isol.	6776	9.87	7	–0.35	1
129-004	S..	15.2	Isol.	6736	9.33	193	–0.08	1
129-009	Sa	15.3	Pair	6415	9.27	24	0.11	1
129-013	S..	15.7	Isol.	6962	9.53	184	–0.03	1
129-016	S..	15.5	N4615 HL	4979	–	–	–	–
129-018	Sc	13.8	N4615 HL	4716	10.05	24	–0.23	1
129-020	Sb	14.8	Isol.	6579	9.50	15	0.14	3
129-021	S..	15.3	Isol.	6697	9.85	24	–1.15	2
129-022	Sab	14.4	Isol.	6972	9.98	2	–0.25	3
129-023	S..	15.7	Isol.	6746	9.41	184	–0.42	4
129-025	Sc	13.5	N4615 HL	4380	10.02	6	0.12	1
130-002	S..	15.6	Isol.	6663	9.61	184	–0.64	1
130-003	Sb	15.4	Isol.	7140	9.04	193	0.68	3
130-005	Sbc	15.5	Isol.	7058	9.30	127	0.21	1
130-006	Sbc	15.0	Isol.	6521	9.33	24	0.04	2
130-008	Sc	14.9	Isol.	7266	9.73	2	–0.53	2
130-009	Sbc	15.3	Pair	6335	9.93	24	–0.03	1
130-012	Sbc	15.2	Pair	7131	9.97	24	0.19	1
130-014	Sbc	15.1	Isol.	7096	9.57	126	0.09	1
130-021	Sa	15.4	Isol.	7163	9.33	127	0.18	1
130-025	Sa	15.5	Isol.	7001	9.68	15	0.02	1
130-026	Sc	15.5	Quadr.	6870	9.85	24	–0.03	1
130-027	Sbc	15.6	Quadr.	6834	9.94	40	–0.13	1
130-029	Sc	15.4	Pair	6560	9.39	193	0.04	1
131-008	Sbc	15.6	Isol.	5972	9.76	88	–0.04	1
131-009	Sc	15.3	Isol.	7522	9.64	24	–0.04	1
157-012	Sbc	15.1	Isol.	6814	9.73	40	–0.19	1
157-032	Sa	15.2	Isol.	6811	9.16	24	0.64	4
157-035	Sb	13.7	Isol.	6281	10.18	24	–0.05	1
157-044	Pec	15.4	Isol.	6607	9.19	193	0.22	1
157-051	Sc	15.3	N4005 HL	5151	9.65	24	–0.04	2

Table 4. continued.

CGCG	Type	m_p mag	Cloud	V km s^{-1}	log M_{HI} $M_\odot$	Ref.	Def$_{HI}$	Qual
157-062	Pec	15.5	Isol.	6882	9.68	5	0.01	2
157-064	Sb	14.8	Isol.	6407	9.84	40	0.02	2
157-075	Sc	15.7	Isol.	6694	9.54	7	0.06	2
157-077	S..	15.4	N4005 HL	4100	–	–	–	–
158-009	Sb	14.0	Pair	7494	9.07	24	0.65	4
158-010	Sbc	15.2	Pair	7930	9.46	24	0.17	2
158-029	S..	14.1	N4169 HL	3836	8.98	22	0.46	2
158-030	Sab	14.6	N4169 HL	3970	9.51	22	–0.35	2
158-031	Sb	13.8	N4169 HL	3825	10.03	39	–0.13	1
158-036	Sb	13.8	Isol.	6532	9.96	2	–0.20	1
158-038	Sab	15.3	Isol.	6725	9.36	40	0.07	1
158-042	S..	14.8	N4169 HL	3868	8.97	88	0.11	2
158-046	S..	15.0	N4169 HL	3848	–	–	–	–
158-047	Sb	13.5	N4169 HL	3903	9.79	39	0.07	1
158-053N	Sa	14.7	Pair	6599	9.79	2	–0.02	1
158-054	Pec	14.6	Isol.	7685	9.76	2	–0.13	3
158-055	Sb	15.3	Isol.	7650	9.53	24	0.46	4
158-056	Sa	15.5	Tripl.	8102	9.53	24	0.16	1
158-061	Sa	13.7	N4169 HL	3876	<8.24	168	0.84	–
158-070	Sbc	15.3	Quadr.	7634	9.58	5	0.23	1
158-081	Pec	14.5	Isol.	6734	9.26	2	–0.03	2
158-091	Sab	15.7	IC3165 G	7607	9.54	2	-0.17	2
158-102	S..	15.7	N4615 HL	4515	9.49	7	0.03	1
158-105	Sbc	15.1	Isol.	6824	9.98	24	–0.16	1
158-112	Sbc	14.4	Pair	7165	9.73	2	0.41	4
159-004	S..	15.7	Pair	7004	9.11	88	0.15	2
159-005	Sbc	14.7	Pair	6996	9.61	2	0.27	2
159-008	Sb	14.6	Isol.	7393	10.03	126	0.06	1
159-009	Sab	14.1	N4615 HL	4551	10.14	24	–0.52	1
159-010	Sb	15.7	Isol.	7009	9.62	5	0.24	1
159-019	Sbc	14.9	N4615 HL	4573	9.62	6	–0.09	1
159-031	Sa	15.3	Pair	7511	9.91	127	–0.16	1
159-033	Sa	15.0	Isol.	7674	9.34	126	0.54	1
159-037	Sab	14.6	Isol.	7291	9.73	126	–0.28	1
159-040	Sa	15.2	Isol.	7019	9.93	24	–0.34	1
159-048	S..	15.5	Isol.	7064	9.53	193	–0.25	1
159-049S	S..	15.7	Pair	6330	–	–	–	–
159-054	Sc	15.5	N4615 HL	4759	9.41	88	–0.01	1
159-055	Sbc	15.6	Pair	7737	10.01	24	0.01	1
159-058	Sa	15.5	Isol.	6797	<9.50	184	>–0.07	–
159-059	Sab	14.5	Isol.	7528	9.76	2	–0.31	2
159-060	Pec	15.5	Isol.	7182	9.67	5	0.04	3
159-061	Sbc	14.8	Isol.	6966	9.49	2	0.28	3
159-064	S..	15.6	Isol.	7265	<9.64	184	>–0.12	–
159-068	Sa	15.7	Isol.	6313	9.25	184	0.03	4
159-071	Sc	15.5	Isol.	6971	9.72	193	–0.03	1
159-072N	Pec	14.8	Pair	6631	10.09	2	–0.03	4
159-072S	Pec	14.8	Pair	6590	10.03	2	–0.12	4
159-076	Sbc	14.5	Isol.	6743	9.51	2	0.39	1
159-080	Sb	15.7	Isol.	6859	9.54	126	0.14	1
159-081	Sbc	15.5	Pair	8116	9.85	40	–0.20	1
159-082	Sc	14.8	Pair	8078	10.01	126	–0.18	1
159-090	Sc	15.5	Tripl.	8315	10.16	126	–0.56	1
159-091	S..	15.1	Isol.	6443	9.16	126	0.00	1
159-092	Sc	14.9	N4615 HL	4754	9.94	126	0.02	1
159-093	Sc	15.3	N4615 HL	5446	<8.58	40	>0.63	5
159-095	Sbc	14.9	Isol.	6837	9.64	2	–0.24	1
159-096	Sc	15.1	Isol.	6186	9.96	126	–0.01	1

Table 4. continued.

CGCG	Type	m_p mag	Cloud	V km s^{-1}	log M_{HI} $M_\odot$	Ref.	Def$_{HI}$	Qual
159-097	Pec	15.4	Isol.	6424	9.02	193	0.21	3
159-101	Pec	15.3	Coma	7745	9.12	6	0.07	1
159-102	Sab	14.5	Coma	7061	9.97	126	–0.25	3
160-001	Sb	15.6	Coma	7945	9.44	88	0.09	1
160-005	Sb	14.8	Isol.	6319	10.06	126	–0.01	1
160-007	S..	15.4	Coma	6462	<8.82	88	>0.74	–
160-009	S..	15.5	Coma	7132	<8.84	193	>0.55	–
160-012	S..	15.7	Isol.	6348	<9.36	184	>–0.16	–
160-015	S..	15.5	Coma	7443	<8.90	40	>0.63	5
160-018	S..	15.3	Coma	7092	<8.82	88	>0.63	–
160-020	Pec	15.5	Coma	4968	8.93	24	0.27	4
160-025	Sa	14.0	Coma	6702	<8.75	27	>0.92	–
160-026	Sc	15.5	Coma	7545	9.29	40	0.23	2
160-031	S..	15.7	Coma	6852	<8.84	6	>0.62	5
160-032	Sb	14.9	Coma	7747	<8.83	2	>0.76	5
160-055	Sab	14.2	Coma	7164	9.34	40	0.49	2
160-058	Sbc	15.5	Coma	7616	9.49	126	0.40	1
160-064	Pec	15.4	Coma	7368	<8.32	132	>0.93	–
160-067	Pec	15.4	Coma	7655	9.34	181	–0.01	2
160-073	Pec	15.1	Coma	5425	8.57	132	0.96	5
160-076	Sc	15.6	Coma	5390	9.64	132	–0.35	5
160-081	Sb	14.7	Coma	5898	<8.86	1	>1.29	5
160-086	Pec	15.4	Coma	7499	8.74	126	0.76	1
160-088	Sb	14.6	Coma	7287	9.35	40	0.42	1
160-095	Sb	13.7	Coma	5482	9.33	126	0.96	1
160-096N	Pec	15.2	Coma	6892	8.42	132	0.95	5
160-098	Pec	15.3	Coma	8762	9.05	1	0.41	2
160-102	Sab	14.8	Coma	7095	9.97	126	–0.01	1
160-106	Pec	15.1	Coma	6876	9.05	132	0.54	5
160-108	Pec	15.5	Coma	8323	<8.29	6	>0.92	5
160-114	S..	15.6	Coma	7454	<8.74	88	>0.81	–
160-121	Sb	15.5	Coma	6676	9.92	126	0.02	1
160-127	Sc	15.5	Coma	5500	9.71	126	–0.10	1
160-128	Pec	15.3	Coma	7920	9.73	193	–0.33	1
160-137	Sa	13.9	Coma	7050	9.79	40	–0.05	1
160-138	S..	15.7	Coma	7861	<8.56	193	>0.71	–
160-139	Pec	15.0	Coma	4749	9.96	126	–0.19	2
160-141	Pec	15.5	Coma	7292	8.95	1	0.32	1
160-146	Sa	15.4	Pair	7385	<8.41	193	>1.12	–
160-148	Sa	14.3	N5056 HL	5988	9.75	126	–0.07	1
160-151	Pec	15.1	N5056 HL	6258	8.97	24	0.31	2
160-152W	Sb	14.0	N5056 HL	5610	9.95	2	0.05	1
160-155	Sb	15.3	N5056 HL	6366	9.60	126	0.04	1
160-156	Sa	15.3	Pair	7262	9.59	24	0.28	1
160-163N	S..	15.7	Isol.	6877	<8.92	24	>0.28	–
160-164	Sc	15.2	N5056 HL	6074	9.69	126	–0.19	1
160-166	Sb	13.6	N5056 HL	6408	9.80	2	0.24	1
160-167	Sb	15.0	N5056 HL	6039	9.75	126	0.02	1
160-168	Sc	14.2	Isol.	7476	10.36	2	–0.40	1
160-169	S..	15.6	Isol.	6850	9.41	193	0.08	1
160-173	Sc	13.6	N5056 HL	5592	10.12	126	–0.12	1
160-175	S..	15.1	N5056 HL	5661	9.25	24	0.18	1
160-180	S..	15.4	N5056 HL	5581	–	–	–	–
160-181	Sc	14.3	N5056 HL	5550	9.87	126	–0.11	1
160-182	Sab	15.0	Isol.	6994	9.62	5	0.07	1
160-183	Pec	14.7	N5056 HL	5605	9.57	40	–0.14	3
160-192	Sb	14.3	Isol.	6649	10.25	126	–0.09	1
160-195	S..	15.7	Tripl.	7247	9.14	193	–0.04	2

Table 4. continued.

CGCG	Type	m_p mag	Cloud	V km s^{-1}	log M_{HI} $M_\odot$	Ref.	Def_{HI}	Qual
160-206	S..	15.6	N5056 HL	5053	8.99	40	0.25	1
160-207	Sc	15.3	N5056 HL	5081	9.71	5	0.05	1
160-209	Pec	15.4	Pair	7168	9.28	24	0.28	2
160-212	Sa	14.9	Coma	7549	8.78	132	0.90	5
160-213	Pec	15.5	Coma	9386	< 8.17	1	>1.11	5
160-243	S..	15.6	Coma	5121	–	–	–	–
160-252	Pec	15.1	Coma	7718	9.01	40	0.56	1
160-257	Sa	14.6	Coma	5821	8.66	132	0.97	5
160-260	Sa	13.7	Coma	7985	9.18	126	0.81	1
160-261	S..	15.6	Coma	6917	<8.56	193	>0.81	–
161-029	Sb	15.7	N5056 HL	4930	–	–	–	–
161-031	Sbc	14.9	Tripl.	7270	9.75	40	0.08	2
161-040	Sc	15.6	Isol.	7260	9.43	40	–0.02	1
161-041	S..	15.5	N5056 HL	4979	8.81	88	0.32	1
161-043	Sa	14.4	Isol.	6638	9.62	24	0.33	2
161-044	Sc	15.3	N5056 HL	4983	9.21	40	0.48	1
161-048	Sa	15.1	Isol.	7280	<8.82	193	>0.72	–
161-051	S..	15.6	Isol.	7150	<9.17	193	>–0.12	–
161-052	Pec	15.1	Isol.	7072	9.46	88	–0.50	2
161-054	Sa	15.5	Isol.	6756	9.41	193	–0.07	1
161-063	Sbc	15.5	Isol.	7300	9.97	88	–0.06	1
161-066	S..	15.7	Isol.	7380	10.12	40	–0.56	3
161-069	Sb	14.6	Isol.	7172	9.88	24	–0.27	1
161-071	Pec	14.9	N5056 L	4827	9.84	5	–0.26	1
161-073	Sb	14.2	Isol.	7320	10.38	24	–0.21	1

1: Giovanelli & Haynes (1985); 2: Chincarini et al. (1983a); 3: Sullivan et al. (1981); 4: Chincarini et al. (1983b); 5: Fontanelli (1984); 6: Bothun et al. (1985); 7: Williams & Kerr (1981); 15: Haynes & Giovanelli (1984); 22: Sulentic & Arp H (1982); 24: Gavazzi (1987); 27: Eder et al. (1991); 39: Lewis et al. (1985); 40: Gavazzi (1989); 43: Salzer et al. (1990); 88: Scodeggio & Gavazzi (1993); 105: Lu et al. (1993); 111: Mould et al. (1995); 126: Haynes et al. (1997); 127: Dell'Antonio et al. (1996); 132: Bravo Alfaro (2001); 168: Magri et al. (1994); 181: Beijsbergen (2003); 184: van Driel et al. (2000); 185: Vogt et al. (2004); 193: This work.

Appendix A: Notes on individual galaxies

CGCG 127-018: Our H I detection ($V_{HI} = 6922 \pm 2$ km s^{-1}, $W_{50} = 147$ km s^{-1} and $I_{HI} = 2.1 \pm 0.06$ Jy km s^{-1}) is consistent with our previous (van Driel et al. 2000) Nançay detection ($V_{HI} = 6936 \pm 16$ km s^{-1}, $W_{50} = 131$ km s^{-1} and $I_{HI} = 2.7 \pm 0.3$ Jy km s^{-1}) and with the Arecibo detection of Gavazzi (1987) at $V_{HI} = 6935$ km s^{-1}.

CGCG 127-039: The integrated line intensity of our H I detection ($V_{HI} = 6911 \pm 1$ km s^{-1}, $W_{50} = 37$ km s^{-1} and $I_{HI} = 0.82 \pm 0.04$ Jy km s^{-1}) is 3.4 times lower than that of our previous Nançay detection (van Driel et al. 2000), with $V_{HI} = 6919 \pm 9$ km s^{-1}, $W_{50} = 40$ km s^{-1} and $I_{HI} = 2.8 \pm 0.2$ Jy km s^{-1}. The latter was made with an elongated $3\farcm6 \times 21'$ ($\alpha \times \delta$)*HPBW*, which is considerably larger than the $3\farcm6$ round Arecibo beam. This difference can be due to the 13.6 *B* mag SBbc spiral NGC 3832, $17\farcm2$ due south of the target galaxy, whose mean H I line parameters ($V_{HI} = 6909 \pm 6$ km s^{-1}, $W_{50} = 171$ km s^{-1} and $I_{HI} = 10.4$ Jy km s^{-1}) are based on 5 spectra, all obtained at Arecibo (Chincarini et al. 1983a; Giovanardi & Salpeter 1985; Lewis 1985; Lewis et al. 1985; Sullivan et al. 1981).

CGCG 127-055: Our H I detection ($V_{HI} = 6626 \pm 3$ km s^{-1}, $W_{50} = 215$ km s^{-1} and $I_{HI} = 1.9 \pm 0.08$ Jy km s^{-1}) is consistent with our previous measurement (van Driel et al. 2000) made at Nançay, with $V_{HI} = 6656 \pm 21$ km s^{-1}, $W_{50} = 183$ km s^{-1} and $I_{HI} = 2.1 \pm 0.3$ Jy km s^{-1}. Our new data have a 3.6 times better rms noise level.

CGCG 128-072: Given the uncertainties, the global parameters of our H I detection ($V_{HI} = 6795 \pm 6$ km s^{-1}, $W_{50} = 119$ km s^{-1} and $I_{HI} = 0.82 \pm 0.07$ Jy km s^{-1}) are consistent with those of our previous Nançay detection (van Driel et al. 2000), with $V_{HI} = 6848 \pm 81$ km s^{-1}, $W_{50} = 213$ km s^{-1} and $I_{HI} = 1.4 \pm 0.6$ Jy km s^{-1}. Our new data have a 5.4 times better rms noise level.

CGCG 129-004: discrepant values for the optical redshift have been published, 4847 and 6729 km s^{-1} (Gavazzi et al. 1999a, and the compilation by Falco et al. 1999); we find an H I value of 6736 ± 7 km s^{-1}, consistent with the latter value.

CGCG 130-003: there are two discrepant literature values for its optical redshift, 7094 and 22,425 km s^{-1} (Straus et al. 1992; Gregory et al. 1988); we find an H I value of 7140 ± 4 km s^{-1}, consistent with the former value.

CGCG 157-044: our H I detection ($V_{HI} = 6607 \pm 4$ km s^{-1}, $W_{50} = 240$ km s^{-1} and $I_{HI} = 0.84 \pm 0.08$ Jy km s^{-1}) has a 1.7 times lower line intensity than our previous Nançay detection (van Driel et al. 2000), with $V_{HI} = 6628 \pm 36$ km s^{-1}, $W_{50} = 309$ km s^{-1} and $I_{HI} = 1.5 \pm 0.4$ Jy km s^{-1}. The difference is less than two times the uncertainty in the latter value, however, and therefore not significant.

CGCG 159-071: the global parameters of our H I detection ($V_{HI} = 6971 \pm 1$ km s^{-1} and $W_{50} = 189$ km s^{-1} and $I_{HI} = 2.6 \pm 0.1$ Jy km s^{-1}) are consistent with those of our previous Nançay detection (van Driel et al. 2000), with $V_{HI} = 6985 \pm 6$ km s^{-1}, $W_{50} = 164$ km s^{-1} and $I_{HI} = 2.4 \pm 0.4$ Jy km s^{-1}.

CGCG 159-097: Its optical redshift, 6573 ± 190 km s^{-1}, is not well determined. We measured an H I value of 6424 ± 30 km s^{-1}, consistent with 3 of the published optical values – only the optical velocity of 6883 ± 75 km s^{-1} measured by van Haarlem et al. (1993) is in disagreement with all other values.

CGCG 160-128: Our detection ($V_{HI} = 7920 \pm 1$ km s^{-1}, $W_{50} = 115$ km s^{-1} and $I_{HI} = 2.5 \pm 0.07$ Jy km s^{-1}) is consistent with our previous Nançay detection ($V_{HI} = 7940 \pm 5$ km s^{-1}, $W_{50} = 100$ km s^{-1} and $I_{HI} = 2.2 \pm 0.3$ Jy km s^{-1}), which was based on data with a 4 times higher rms of 2.8 mJy (van Driel et al. 2000).

CGCG 161-051: We did not confirm our previous, quite tentative Nançay detection (van Driel et al. 2000), with $V_{HI} = 6993$: km s^{-1}, $W_{50} = 235$: km s^{-1} and $I_{HI} = 1.5$: Jy km s^{-1}. Our new spectrum has a 2.4 times better rms, of 1.5 mJy.

CGCG 161-054: Our detection ($V_{HI} = 6756 \pm 3$ km s^{-1}, $W_{50} = 284$ km s^{-1} and $I_{HI} = 1.3 \pm 0.1$ Jy km s^{-1}) is consistent with our previous, tentative Nançay detection, with $V_{HI} = 6760$: km s^{-1}, $W_{50} = 335$: km s^{-1} and $I_{HI} = 1.8$: Jy km s^{-1}, which was based on data with a 4 times higher rms of 3.2 mJy (van Driel et al. 2000).

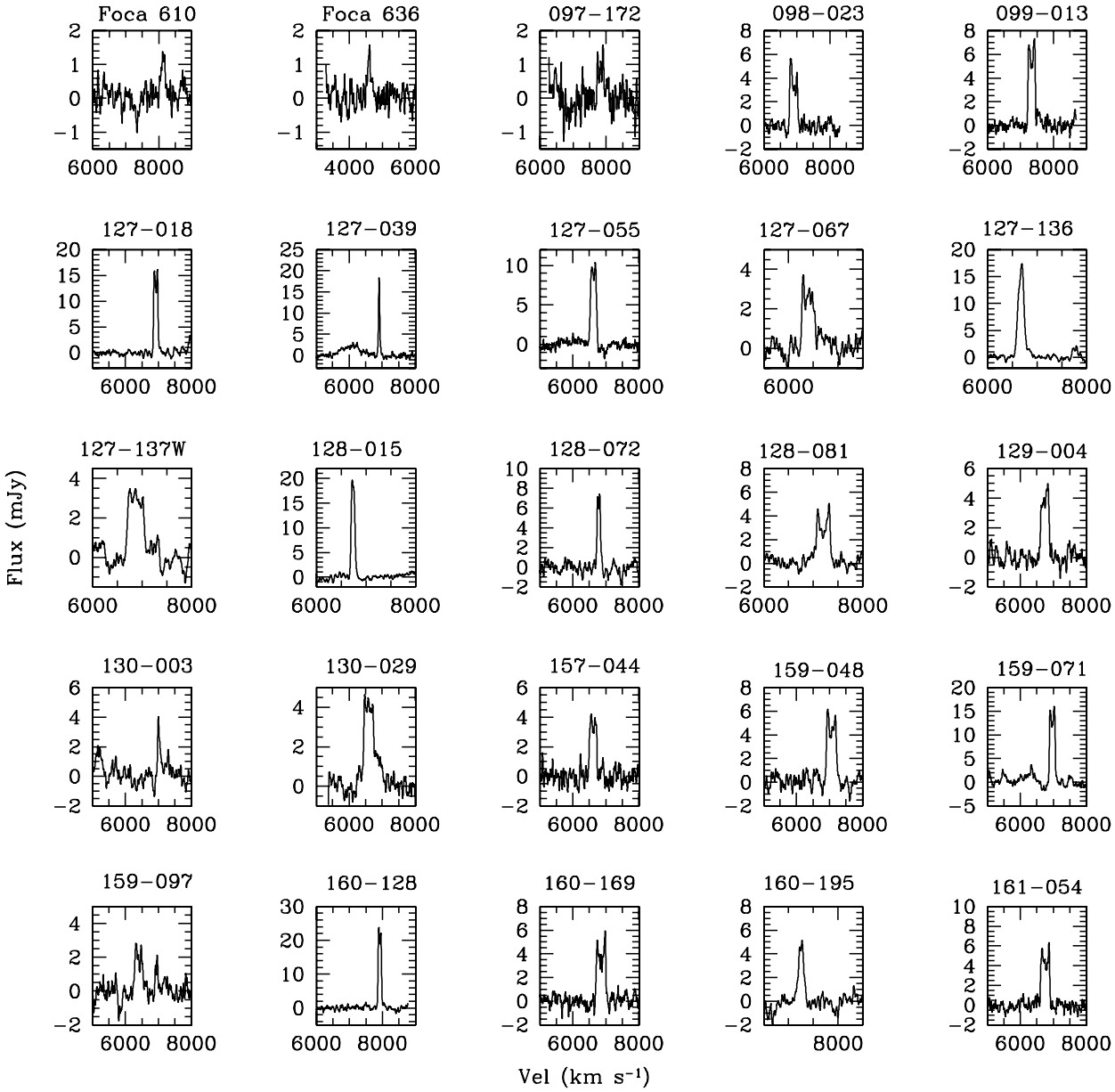

Fig. A.1. H I spectra of the tentatively detected galaxies in the Coma Supercluster.

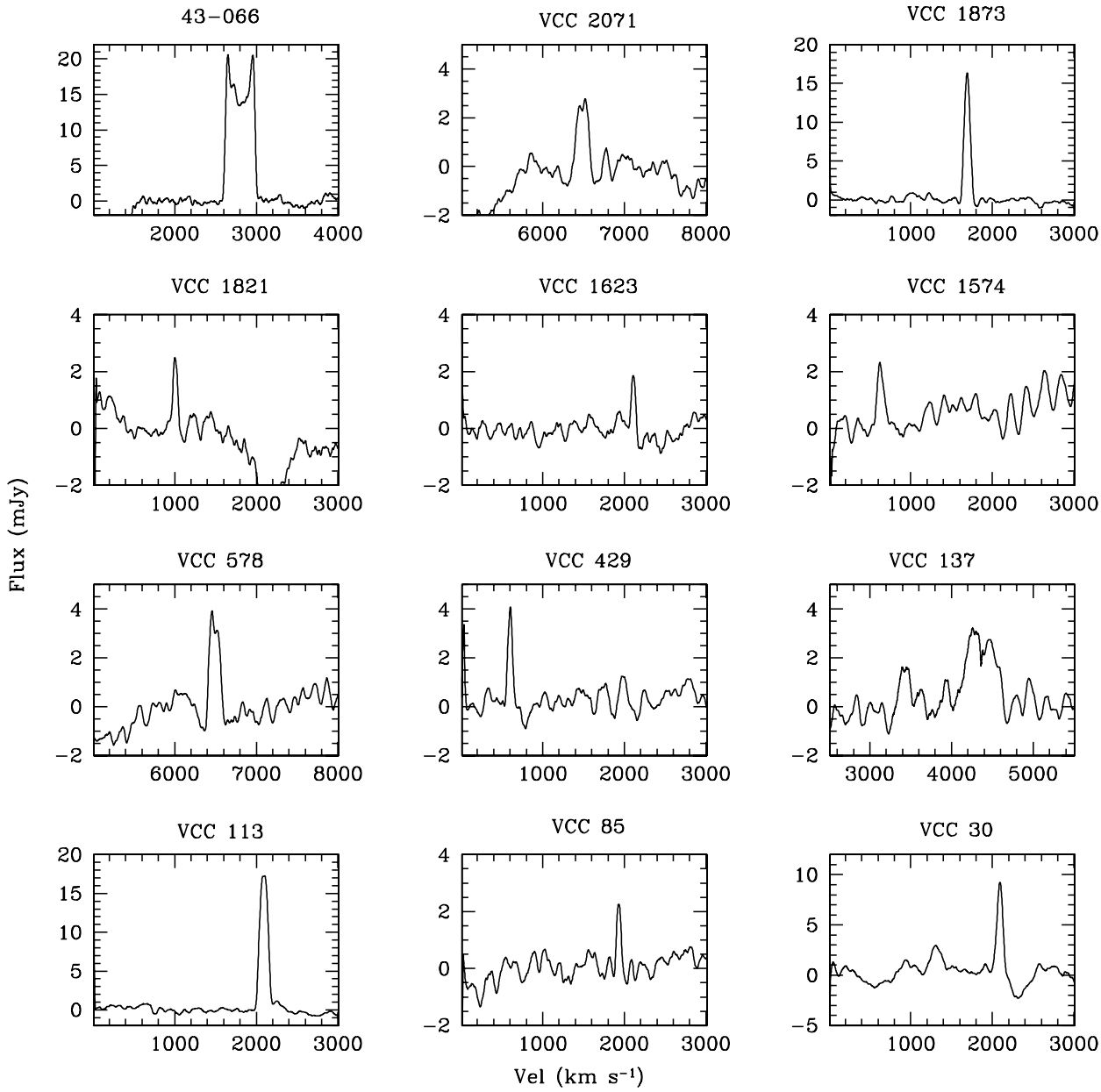

Fig. A.2. H I spectra of the tentatively detected galaxies in the Virgo cluster.